

Research Report

Nanocomposite of Al_2O_3 and $\text{ZrO}_2\text{-TiO}_2$ as a Support for NO_x Storage-reduction Catalyst

Haruo Imagawa

Report received on July 6, 2011

■ABSTRACT■ A nanocomposite of $\gamma\text{-Al}_2\text{O}_3$ and $\text{ZrO}_2\text{-TiO}_2$ (AZT) was synthesized for thermal stability by the coprecipitation method. XRD and TEM results indicated that primary particles of $\gamma\text{-Al}_2\text{O}_3$ and a solid solution of $\text{ZrO}_2\text{-TiO}_2$ coexisted as secondary particles. After thermal treatment, sintering of the $\text{ZrO}_2\text{-TiO}_2$ particles was inhibited relative to that in the physical mixture of Al_2O_3 and $\text{ZrO}_2\text{-TiO}_2$ powder. This was attributed to the diffusion barrier (against $\text{ZrO}_2\text{-TiO}_2$) created by Al_2O_3 primary particles in AZT. Consequently, NO_x storage-reduction catalyst containing AZT had a larger NO_x storage amount than the catalyst containing the physically mixed oxide after a thermal aging test.

Ti doped AZT (Ti-AZT) was synthesized based on AZT in order to achieve sulfur durability, as well as thermal stability. Ti-AZT maintained the original AZT structure and exhibited lower basicity after the Ti doping step. Doped titanium was homogeneously distributed on the surface without the formation of discrete TiO_2 particles. SO_2 -temperature programmed desorption at less than 823 K indicated that the catalyst containing Ti-AZT had larger sulfur desorption than that containing AZT, which provided a large NO_x storage amount after sulfur aging tests.

■KEYWORDS■ NO_x Storage-reduction Catalyst, Nanocomposite, Solid Solution, Titanium Doping, Thermal Stability, Sulfur Durability, Alumina, Zirconia, Titania

1. Introduction

In order to minimize emissions of greenhouse gases into the global environment, a reduction in carbon dioxide (CO_2) emissions from automobiles is urgently required. In addition, it is also necessary to make the most efficient use of the limited fossil resources available. The lean-burn engine system is one of the most attractive methods to reduce fuel consumption. However, in this system, conventional three-way catalysts cannot reduce nitrogen oxides (NO_x) into nitrogen (N_2) due to the presence of excess oxygen in the exhaust gases. Hence, a variety of catalyst systems have been studied for the reduction of NO_x in lean systems.⁽¹⁻³⁾

The NO_x storage-reduction catalyst (NSR catalyst) has been developed as a promising feasible solution for NO_x removal from lean-burn engines.⁽⁴⁻⁶⁾ Toyota first applied this system to a commercial lean-burn gasoline engine in 1994.^(4,7) The mechanism of NO_x storage and reduction reaction is shown in Fig. 1. Firstly, during the lean condition, excess NO_x is oxidized to NO_2 on precious metal catalysts and stored in the form of nitrate within the storage materials. Secondly, when the engine is switched to operate on a rich air-fuel ratio (A/F), the nitrates stored in the

storage materials are reduced to N_2 by hydrogen (H_2), carbon monoxide (CO), and hydrocarbons (HC).

Although the NSR catalyst brings various practical benefits, it has two main technical problems: sulfur poisoning and thermal deterioration. Sulfur dioxide (SO_2) in the gas exhaust reacts with the storage materials and forms sulfates.⁽⁸⁻¹²⁾ Recent studies on sulfur durability in catalysts have revealed that TiO_2 in support materials provides a high tolerance against sulfur poisoning due to its high acidity/low basicity.^(8,13-16)

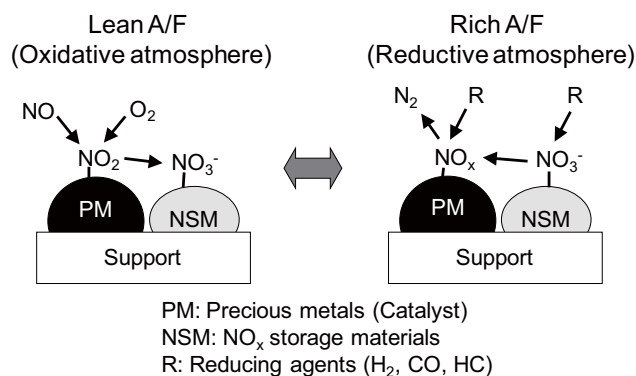


Fig. 1 NO_x purification mechanism on NSR catalysts.

Thermal deterioration of the catalyst occurs due to both solid-phase reaction of NO_x storage materials with TiO_2 ⁽¹⁷⁾ and aggregation of the support particles.⁽¹⁸⁾

In an effort to avoid solid-phase reaction, ZrO_2 is typically added as a $\text{ZrO}_2\text{-TiO}_2$ solid solution.^(13,15) On the other hand, Al_2O_3 , which has excellent thermal stability, is also added to the support. Typically, Al_2O_3 is physically mixed with the other support materials, and does not contribute to the thermal stability of the other support components.

The design of a novel nanocomposite of Al_2O_3 and $\text{ZrO}_2\text{-TiO}_2$ (AZT) as a support for NSR catalysts is proposed to inhibit the thermal aggregation of $\text{ZrO}_2\text{-TiO}_2$ primary particles, as a result of the Al_2O_3 primary particles providing a diffusion barrier.^(15,19) In this nanocomposite, primary particles of Al_2O_3 and $\text{ZrO}_2\text{-TiO}_2$ coexist within the same secondary particle, which may allow the Al_2O_3 particles to act as a diffusion barrier to the $\text{ZrO}_2\text{-TiO}_2$ particles (**Fig. 2**). Concerning sulfur durability, the presence of TiO_2 in Al_2O_3 as well as ZrO_2 may actively enhance sulfur durability. Therefore, the NSR catalyst containing AZT as a support is expected to exhibit not only excellent thermal stability, but also higher sulfur durability, because all of the particles contain TiO_2 .

In this review, the effect of AZT on the thermal stability of the powder and catalyst is investigated in Section 2. Then, the effect of titanium doping (TiO_2 onto AZT) on sulfur durability is discussed in Section 3.

2. Effect of AZT on Thermal Stability as a Support for NSR Catalyst⁽²⁰⁾

2.1 Synthesis and Characterization of AZT

AZT was prepared by a conventional coprecipitation method.⁽²⁰⁾ The mole ratio of $\text{Al}_2\text{O}_3\text{:ZrO}_2\text{:TiO}_2$ was 50:30:20 (mol%). The XRD pattern of AZT after calcination at 1073 K is shown in **Fig. 3(a)**. AZT consists of an amorphous $\gamma\text{-Al}_2\text{O}_3$ phase and a crystalline tetragonal ZrO_2 phase. The peak assigned to tetragonal ZrO_2 (101) phase shifted from $2\theta = 30.22^\circ$ to 30.42° , which suggests that TiO_2 has become dissolved in the ZrO_2 phase and a $\text{ZrO}_2\text{-TiO}_2$ solid solution has been successfully formed in this synthetic step.

A TEM image of AZT is shown in **Fig. 4(a)**. Primary particles of Al_2O_3 (pale gray particles) and $\text{ZrO}_2\text{-TiO}_2$ (dark gray and clear particles) coexisted in the same secondary particles. Each of the primary particles was less than 20 nm. This nanocomposite structure is attributed to the conditions under which precipitation of Al_2O_3 and $\text{ZrO}_2\text{-TiO}_2$ begins to develop at the same time.

Table 1 shows the BET surface area at 1073 K. AZT had almost the same surface area as a physical mixture of Al_2O_3 and $\text{ZrO}_2\text{-TiO}_2$ (physically mixed oxide), of approximately $130 \text{ m}^2/\text{g}$. Pure $\text{ZrO}_2\text{-TiO}_2$ showed a sharp drop in the surface area between 873 and 973 K

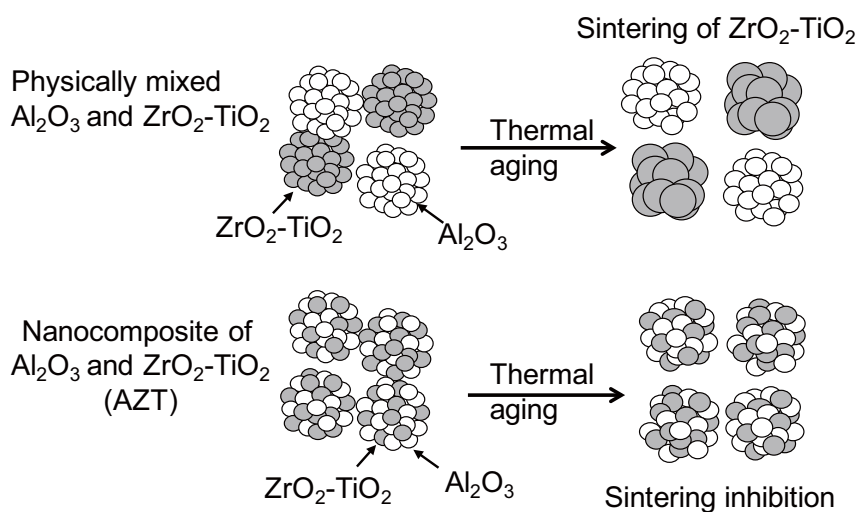


Fig. 2 Concept chart of AZT.

due to the rapid crystallization and sintering of ZrO_2 - TiO_2 . However, AZT showed only a gradual decrease in the surface area without any sharp drops throughout the heating, which has been reported in the literature in more detail.⁽²⁰⁾ This trend indicates that the Al_2O_3 particles act as a diffusion barrier for the

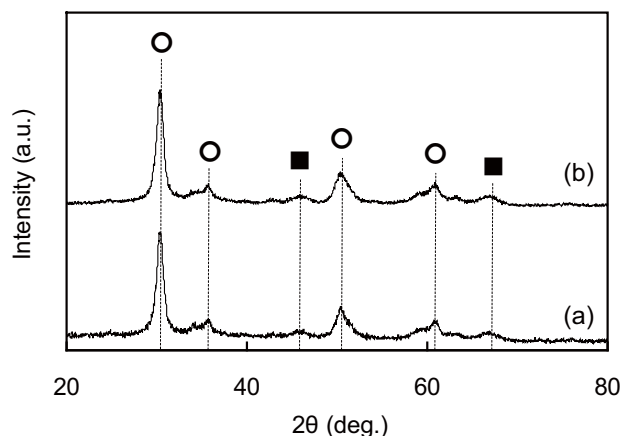


Fig. 3 XRD patterns of (a) AZT and (b) Ti-AZT calcined at 1073 K. (○) tetragonal ZrO_2 ; (■) γ - Al_2O_3 .

ZrO_2 - TiO_2 particles in AZT, which prevents rapid sintering of the ZrO_2 - TiO_2 particles.

With regards to the pore diameter distribution, AZT exhibited a single sharp mesopore around 15 nm (**Fig. 5**, black line). Al_2O_3 and ZrO_2 - TiO_2 are present in the same secondary particle, which has only one pore size. This pore diameter distribution is in good agreement with the AZT structure. On the other hand, the physically mixed oxide had a broad pore distribution from 9 nm to 40 nm (**Fig. 5**, gray line). This broad distribution results from the combination of two different pore sizes derived from the Al_2O_3 secondary particle and the ZrO_2 - TiO_2 secondary particle. After calcination of the physically mixed oxide at 1073 K, the two characteristic peaks became distinct (**Fig. 5**, black broken line). The mesopore volume after calcination at 1073 K is also shown in **Table 1**. AZT had a larger mesopore volume than the physically mixed oxide, because ZrO_2 - TiO_2 particles in AZT were inhibited from aggregating and maintained a large spacing among the primary particles.

It has been reported that TiO_2 in supports has a high

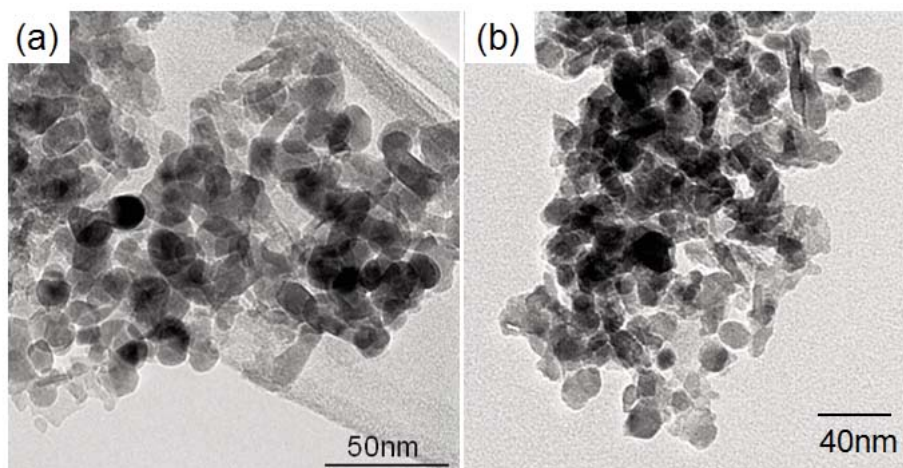


Fig. 4 FE-TEM micrographs of (a) AZT and (b) Ti-AZT calcined at 1073 K.

Table 1 BET surface area, base amount, and mesopore volume of samples after calcination at 1073 K.

	BET surface area (m^2/g)	Base amount ($\mu mol/g$)	Mesopore volume (cm^3/g)
AZT	128	2.7	0.415
Ti-AZT	112	2.1	0.410
Physically mixed oxide	130	12.1	0.318

tolerance against sulfur poisoning, because TiO_2 is an acidic oxide.⁽⁸⁾ TiO_2 is incorporated as a $\text{ZrO}_2\text{-TiO}_2$ solid solution in AZT. Table 1 shows the amount of base as determined by CO_2 temperature programmed desorption (TPD) measurements. The amount of base in AZT was one-fifth the amount of that in the physically mixed oxide. This result suggests the possibility of inhibition of SO_x adsorption on the surface in NSR catalysts using AZT as a support.

The amount of CO_2 adsorbed onto $\text{ZrO}_2\text{-TiO}_2$ is almost negligible.⁽¹³⁾ Therefore, the difference in basicity between AZT and the physically mixed oxide

originates from the Al_2O_3 state. In the physically mixed oxide, CO_2 is easily adsorbed onto the basic surface of the Al_2O_3 particles because of the presence of pure Al_2O_3 secondary particles. On the other hand, in AZT, it can be inferred that the basicity of Al_2O_3 was decreased due to the presence of trace amounts of TiO_2 as an impurity, because TiO_2 has a high acidity and negligible basicity. The AZT was synthesized by coprecipitation, which makes it possible that trace amounts of Ti are present on the surface of the Al_2O_3 particles. Thus, the acidity of TiO_2 may cancel out the basicity of Al_2O_3 to some degree. To clarify this point, further experiments were performed and the data is shown in Section 3.1.

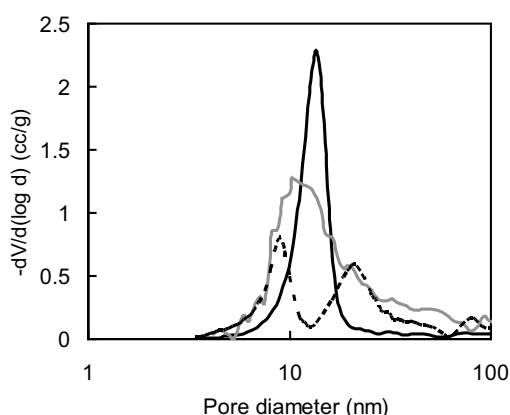


Fig. 5 Pore distribution of samples: AZT calcined at 1073 K (—), Physically mixed Al_2O_3 calcined at 1073 K and $\text{ZrO}_2\text{-TiO}_2$ calcined at 773 K (---), Physically mixed Al_2O_3 and $\text{ZrO}_2\text{-TiO}_2$ calcined at 1073 K (----).

2.2 Thermal Stability of $\text{ZrO}_2\text{-TiO}_2$ Particles in AZT

AZT was heated at 1073, 1173, and 1273 K in air, and the average particle size for $\text{ZrO}_2\text{-TiO}_2$ was determined by XRD, as shown in **Fig. 6(a)**. The average particle size of $\text{ZrO}_2\text{-TiO}_2$ in AZT was smaller than that in the physically mixed oxide at each temperature. At 1273 K, the $\text{ZrO}_2\text{-TiO}_2$ particle size in AZT was about half the size of that in the physically mixed oxide. TEM images after thermal treatment at 1173 K also indicate that the particle size of the primary $\text{ZrO}_2\text{-TiO}_2$ particles in AZT was kept small (**Fig. 6(b)**), although obvious sintering of the $\text{ZrO}_2\text{-TiO}_2$ particles could be observed in the physically mixed oxide (**Fig. 6(c)**).

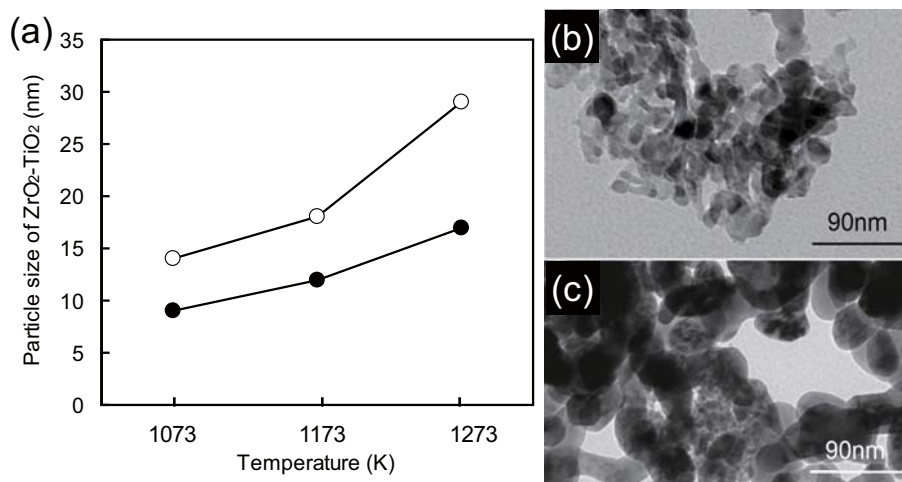


Fig. 6 (a) Average particle size of $\text{ZrO}_2\text{-TiO}_2$ determined by XRD data as a function of the thermal treatment temperature. (●) AZT; (○) Physically mixed oxide. FE-TEM micrographs of (b) AZT and (c) Ti-AZT after thermal treatment at 1173 K.

ZrO₂-TiO₂ primary particles in AZT are surrounded by Al₂O₃ primary particles, which serve as a diffusion barrier for ZrO₂-TiO₂. Consequently, aggregation and sintering of ZrO₂-TiO₂ primary particles by heating are inhibited in AZT in accordance with the schematic shown in Fig. 2.

2.3 Catalytic Application of AZT

Taking advantage of nanocomposite structure for thermal stability, AZT was applied as a support for a NO_x storage-reduction catalyst. The catalysts were composed of platinum and rhodium as precious metals, and barium and potassium oxides as NO_x storage materials. Samples were exposed to periodic cycles of lean/rich atmospheres at 1073 K in a thermal aging test,⁽²⁰⁾ which simulates the actual engine exhaust gases. The lean atmosphere for NO_x storage was composed of 11% CO₂, 6.6% O₂, 0.02% C₃H₆, 800 ppm NO, and 3% H₂O in He, and the rich atmosphere of 11% CO₂, 5.6% CO, 1.9% H₂, 0.11% C₃H₆, 50 ppm NO, and 3% H₂O in He. The amount of NO_x storage at each temperature after the thermal aging test is shown in Fig. 7. The gas composition used for the NO_x storage measurement⁽²⁰⁾ was the same as that used in the thermal aging test. The catalyst containing AZT (AZT catalyst) exhibited a larger amount of NO_x storage than that containing the physically mixed oxide (physically mixed catalyst). Specifically, the NO_x storage of the AZT catalyst was twice as large as that of the physically mixed catalyst at 673 K.

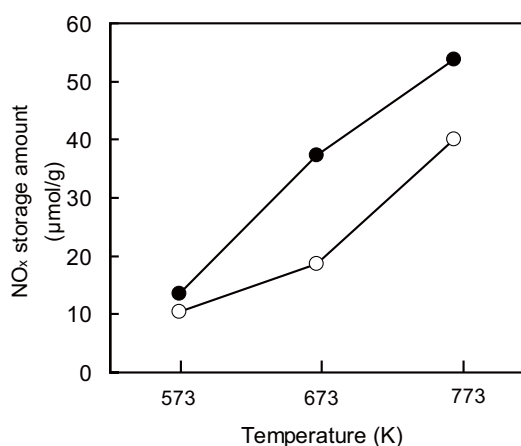


Fig. 7 NO_x storage performance after thermal aging test as a function of the reaction temperature.
(●) AZT catalyst; (○) physically mixed catalyst.

The aggregation and deterioration of precious metals are expected to be inhibited in AZT relative to those in physically mixed oxides. In CO pulse chemisorption measurements probing the noble metal dispersion of the catalysts, it was found that the dispersion of the AZT catalyst was 2.5% and that of the physically mixed catalyst was 1.3% after the thermal aging test, which indicates that the AZT catalyst has a higher density of catalytically active sites after the thermal aging test than the physically mixed catalyst.

For practical purposes, a NO_x storage-reduction catalyst is mainly exposed to temperatures around 673 K,⁽²¹⁾ that is, AZT is a promising support for high performance processing of real exhaust gases from lean-burn engines.

3. Ti-doping in AZT for Sulfur Durability as a Support for NSR Catalyst⁽²²⁾

3.1 Effect of AZT on Sulfur Desorption

As described in Section 2.1, AZT has low basicity, which may result from the presence of a small amount of TiO₂ on Al₂O₃. In energy dispersive X-ray (EDX) analysis of a random sample of Al₂O₃ primary particles, Ti was identified in each of the analysis spots on AZT. Zr was also detected in several spots, but the amount of Zr was smaller than that of Ti. Therefore, small amounts of Ti tend to be present on the Al₂O₃ primary particles due to the coprecipitation synthesis. This support structure suggests that it is possible to inhibit the adsorption of SO_x onto the surface. The desorption of sulfur compounds will also be easily promoted under the rich condition after SO_x adsorption onto the surface.⁽²³⁾

To confirm the effect of the presence of TiO₂ on Al₂O₃ on the sulfur durability, catalysts were exposed to an atmosphere composed of 400 ppm SO₂, 6.6% O₂, and 3% H₂O in N₂ in a sulfur aging test, before subsequent observation of the desorption of sulfur from the catalysts under an atmosphere composed of 11% CO₂, 5.6% CO, 1.9% H₂, 0.34% C₃H₆, 50 ppm NO, and 3% H₂O in N₂ at a fixed temperature. **Figure 8** shows the amounts of sulfur desorption at each measured temperature. The AZT catalyst exhibited a larger amount of sulfur desorption than the physically mixed catalyst for all temperatures, because SO₂ adsorbed onto the AZT catalyst is easily desorbed at a low temperature, owing to the lower basicity resulting from the presence of TiO₂ on the Al₂O₃ surface.

3.2 Synthesis and Characterization of Ti-AZT

On the basis of the results shown in Section 3.1, a titanium-doped AZT (Ti-AZT) was conceptualized and synthesized in order to enhance the total sulfur durability by decreasing the basicity. A concept chart of Ti-AZT is shown in Fig. 9. The purpose of this synthesis is to obtain surface modification via homogeneous distribution of TiO_2 . Therefore, Ti-AZT was synthesized by impregnating AZT with a titanium salt solution.⁽²²⁾ The amount of Ti doped onto the surface was 3.3 at.% based on the metal atom composition of Ti-AZT. Figure 4(b) shows a TEM image of Ti-AZT. Primary particles of Al_2O_3 and $\text{ZrO}_2\text{-TiO}_2$ coexisted in the same secondary particles as seen in AZT. No discrete TiO_2 particles were observed in Ti-AZT. This indicates that Ti is present homogeneously on the AZT surface and may be dissolved in the Al_2O_3 phase as an $\text{Al}_2\text{O}_3\text{-TiO}_2$ solid solution. Some of the impregnated TiO_2 is also dissolved in the $\text{ZrO}_2\text{-TiO}_2$ solid solution, because the synthesis method involves the impregnation of AZT with a Ti salt solution.

EDX analysis of a random sample of Al_2O_3 primary particles revealed that the Ti concentration was more than 10 at.% at each analysis spot on Ti-AZT. Therefore, the surface of the Al_2O_3 particle was modified with Ti in a dispersed state, and this surface localization is expected to work effectively for sulfur resistance. The XRD pattern of Ti-AZT is shown in Fig. 3(b). Ti-AZT exhibits a $\gamma\text{-Al}_2\text{O}_3$ phase and a

tetragonal ZrO_2 phase with a peak shift in the (101) peak due to formation of the $\text{ZrO}_2\text{-TiO}_2$ solid solution, which is the same structure as that observed for AZT. The peak derived from TiO_2 was not observed, which indicates that Ti is doped in the AZT as $\text{Al}_2\text{O}_3\text{-TiO}_2$ and $\text{ZrO}_2\text{-TiO}_2$ without forming discrete TiO_2 .

In the $\text{CO}_2\text{-TPD}$ measurements, the amount of base in Ti-AZT was reduced by 25% relative to that in AZT, and by more than 80% relative to that in the physically mixed oxide (Table 1). The amount of base is in good inverse proportion to the amount of Ti on Al_2O_3 . Consequently, the basicity of Al_2O_3 is canceled out by the acidic TiO_2 , and the increased presence of TiO_2 is effective in further lessening the affinity of the catalyst support to acidic gases. With regards to specific surface area and pore diameter distribution, Ti-AZT maintained the original AZT properties. Moreover, the particle size of $\text{ZrO}_2\text{-TiO}_2$ in Ti-AZT after thermal aging at 1073, 1173 and 1273 K in air was almost identical to that in AZT, which indicates that Ti-AZT has the same thermal stability as AZT, and is expected to exhibit high NO_x storage performance in terms of not only sulfur durability, but also thermal stability.

3.3 Catalytic Application of Ti-AZT

The inhibition of SO_x adsorption and the promotion of sulfur species desorption are required to improve the sulfur durability of NSR catalysts. A catalyst containing Ti-AZT (Ti-AZT catalyst) as a support, platinum and rhodium as precious metals, and barium and potassium as NO_x storage materials was prepared. Samples were exposed to an atmosphere composed of 400 ppm SO_2 , 6.6% O_2 , and 3% H_2O in N_2 for sulfur adsorption, and then the $\text{SO}_2\text{-TPD}$ was examined at temperatures from 623 to 1023 K under an atmosphere composed of 11% CO_2 , 5.6% CO , 1.9% H_2 , 0.34% C_3H_6 , 50 ppm NO , and 3% H_2O in N_2 , as shown in

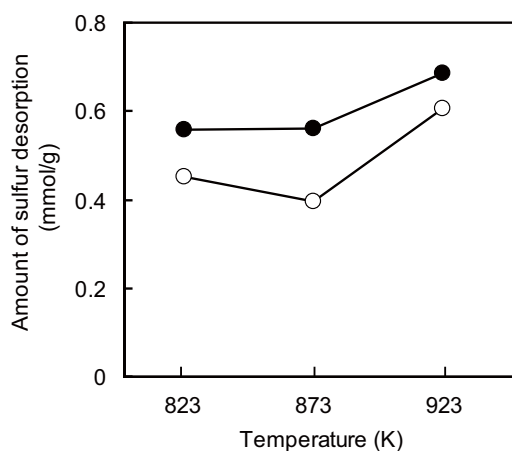


Fig. 8 Amount of sulfur desorption from NSR catalysts at a fixed temperature.
(●) AZT catalyst; (○) physically mixed catalyst.

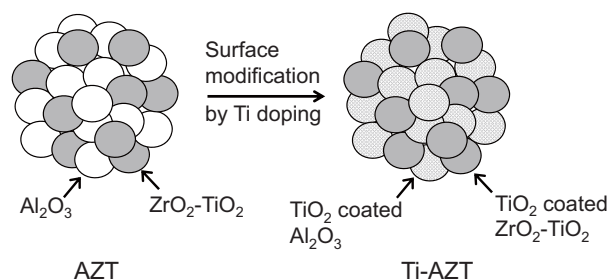


Fig. 9 Concept chart of Ti-AZT.

Fig. 10. The Ti-AZT catalyst exhibits a larger amount of sulfur desorption at low temperatures (around 750 K) than the AZT catalyst. In addition, the starting temperature of sulfur desorption from the Ti-AZT catalyst is 700 K, which is approximately 20 K lower than that from the AZT catalyst. Sulfur species are known to desorb from γ - Al_2O_3 surfaces at less than 873 K⁽⁸⁾; thus, it was determined that the Ti-AZT catalyst facilitates sulfur desorption from the support.

The sulfur concentration of the Ti-AZT catalyst was low from 823 to 980 K in Fig. 10, which indicates that the amount of sulfur attributable to the sulfur-poisoned NO_x storage materials is small in the Ti-AZT catalyst. Moreover, it was also found that the SO_2 -aged Ti-AZT catalyst had a smaller amount of deposited sulfur than the AZT catalyst.⁽²²⁾ Therefore, a close relationship between the following two kinds of sulfur poisoning is suggested: 1) sulfur coverage resulting from SO_x adsorption on the catalysts, and 2) sulfate formation on the NO_x storage materials. The inhibition of SO_x adsorption may bring about inhibition of sulfate formation of the neighboring NO_x storage materials, considering that the main improvement in this novel support is the lowered basicity.

To verify the effect of the Ti-AZT catalyst on sulfur durability in operation as a NSR catalyst, the NO_x storage of the catalysts after the sulfur aging test at 873 K was measured under the same gas conditions as described in Section 2.3. These catalysts were pretreated at 873 K under a rich atmosphere before the NO_x storage measurements. **Figure 11** shows the amount of NO_x storage at each temperature measured. The Ti-AZT catalyst exhibits a larger amount of NO_x

storage than the AZT catalyst. This difference results from a reduction not only in the affinity of the catalyst surface with SO_2 , but also in the amount of sulfur-poisoned NO_x storage materials, as mentioned above.

NSR catalysts continuously suffer from SO_x poisoning as well as thermal deterioration in the flow of actual exhaust gases from lean-burn engines. Ti-AZT has acquired sulfur durability in addition to the thermal-stability characteristics of the original AZT support. Therefore, Ti-AZT is an ideal material for practical use as a NSR catalyst support.

4. Conclusions

AZT was synthesized based on the diffusion barrier concept. After thermal treatment, sintering of ZrO_2 - TiO_2 particles in AZT was inhibited relative to that in physically mixed Al_2O_3 and ZrO_2 - TiO_2 . This is because the Al_2O_3 particles were successfully acting as a diffusion barrier to ZrO_2 - TiO_2 particles in AZT. After a thermal aging test using simulated model exhaust gas from lean-burn engines, the AZT catalyst exhibited a larger amount of NO_x storage than the physically mixed catalyst.

Ti-AZT was synthesized by Ti-doping in AZT as a strategy to provide AZT with sulfur durability. All Al_2O_3 primary particles analyzed in the Ti-AZT had a higher Ti concentration than those in AZT. Ti-AZT maintains the original AZT structure with thermal stability after Ti doping, and provides a support with

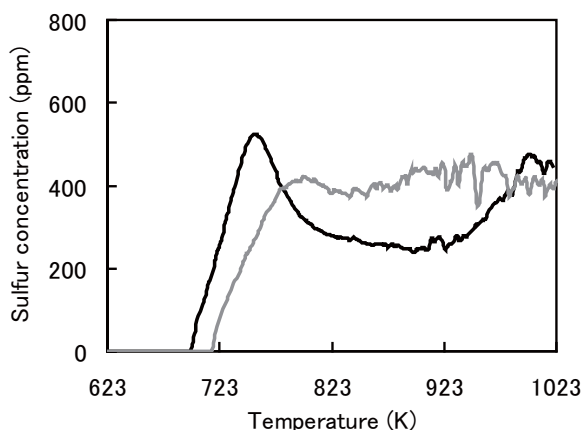


Fig. 10 Sulfur desorption spectra of samples.
Ti-AZT catalyst (—); AZT catalyst (---).

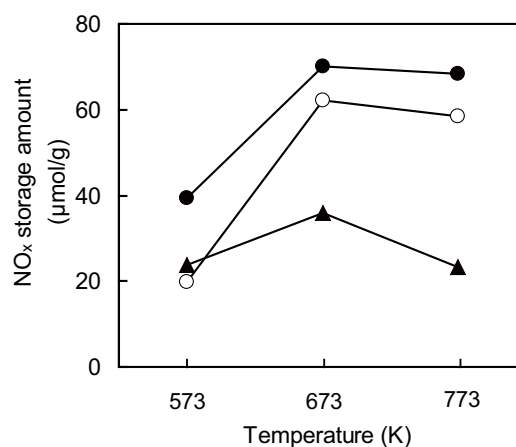


Fig. 11 NO_x storage performance after sulfur aging test as a function of the reaction temperature.
(●) Ti-AZT catalyst; (○) AZT catalyst;
(▲) physically mixed catalyst.

low basicity. In the SO₂-TPD measurements, the Ti-AZT catalyst promotes significant sulfur desorption relative to the AZT catalyst. In addition, the Ti-AZT catalyst exhibits a larger amount of NO_x storage than the AZT catalyst even after sulfur aging tests.

In summary, Ti-AZT has acquired sulfur durability and maintained the thermal stability of the original AZT support, thereby meeting the requirements for NSR catalysts.

References

- (1) Sato, S., Yu-u, Y., Yahiro, H., Mizuno, N. and Iwamoto, M., *Appl. Catal.*, Vol.70 (1991), pp.L1-L5.
- (2) Kintaichi, Y., Hamada, H., Tabata, M., Sasaki, M. and Ito, T., *Catal. Lett.*, Vol.6 (1990), pp.239-244.
- (3) Burch, R. and Millington, P. J., *Catal. Today*, Vol.26 (1995), pp.185-206.
- (4) Miyoshi, N., Matsumoto, S., Katoh, K., Tanaka, T., Harada, J., Takahashi, N., Yokota, K., Sugiura, M. and Kasahara, K., *SAE Tech. Pap. Ser.*, No.950809 (1995)
- (5) Bögner, W., Krämer, M., Krutzsch, B., Pischinger, S., Voigtländer, D., Wenninger, G., Wirbeleit, F., Brogan, M. S., Brisley, R. J. and Webster, D. E., *Appl. Catal. B: Environ.*, Vol.7 (1995), pp.153-171.
- (6) Takahashi, N., Shinjoh, H., Iijima, T., Suzuki, T., Yamazaki, K., Yokota, K., Suzuki, H., Miyoshi, N., Matsumoto, S., Tanizawa, T., Tanaka, T., Tateishi, S. and Kasahara, K., *Catal. Today*, Vol.27 (1996), pp.63-69.
- (7) Matsumoto, S., *Catal. Today*, Vol.29 (1996), pp.43-45.
- (8) Matsumoto, S., Ikeda, Y., Suzuki, H., Ogai, M. and Miyoshi, N., *Appl. Catal. B: Environ.*, Vol.25 (2000), pp.115-124.
- (9) Corbos, E. C., Courtoins, X., Bion, N., Marecot, P. and Duprez, D., *Appl. Catal. B: Environ.*, Vol.80 (2008), pp.62-71.
- (10) Wei, X., Liu, X. and Deeba, M., *Appl. Catal. B: Environ.*, Vol.58 (2005), pp.41-49.
- (11) Dawody, J., Skoglundh, M., Olsson, L. and Fridell, E., *Appl. Catal. B: Environ.*, Vol.70 (2007), pp.179-188.
- (12) Liu, Z. and Anderson, J., *J. Catal.*, Vol.228 (2004), pp.243-253.
- (13) Takahashi, N., Suda, A., Hachisuka, I., Sugiura, M., Sobukawa, H. and Shinjoh, H., *Appl. Catal. B: Environ.*, Vol.72 (2006), pp.187-195.
- (14) Yamamoto, K., Kikuchi, R., Takeguchi, T. and Eguchi, K., *J. Catal.*, Vol.238 (2006), pp.449-457.
- (15) Kanazawa, T., *Catal. Today*, Vol.96 (2004), pp.171-177.
- (16) Ito, K., Kakino, S., Ikeue, K. and Machida, M., *Appl. Catal. B: Environ.*, Vol.74 (2007), pp.137-143.
- (17) Casapu, M., Grunwaldt, J., Maciejewski, M., Wittrock, M., Göbel, U. and Baiker, A., *Appl. Catal. B: Environ.*, Vol.63 (2006), pp.232-242.
- (18) Adams, K. M. and Graham, G. W., *Appl. Catal. B: Environ.*, Vol.80 (2008), pp.343-352.
- (19) Morikawa, A., Suzuki, T., Kanazawa, T., Kikuta, K., Suda, S. and Shinjoh, H., *Appl. Catal. B: Environ.*, Vol.78 (2008), pp.210-221.
- (20) Imagawa, H., Tanaka, T., Takahashi, N., Matsunaga, S., Suda, A. and Shinjoh, H., *J. Catal.*, Vol.251 (2007), pp.315-320.
- (21) Takeuchi, M. and Matsumoto, S., *Top. Catal.*, Vol.28 (2004), pp.151-156.
- (22) Imagawa, H., Tanaka, T., Takahashi, N., Matsunaga, S., Suda, A. and Shinjoh, H., *Appl. Catal. B: Environ.*, Vol.86 (2009), pp.63-68.
- (23) Huang, H. Y., Long, R. Q. and Yang, R. T., *Appl. Catal. B: Environ.*, Vol.33 (2001), pp.127-136.

Figs. 2, 4(a) and 5-7

Reprinted from *J. Catal.*, Vol.251 (2007), pp.315-320, Imagawa, H., Tanaka, T., Takahashi, N., Matsunaga, S., Suda, A. and Shinjoh, H., Synthesis and Characterization of Al₂O₃ and ZrO₂-TiO₂ Nano-composite as a Support for NO_x Storage-reduction Catalyst, © 2007 Elsevier, with permission from Elsevier.

Figs. 4(b), 8, 10 and 11

Reprinted from *Appl. Catal. B: Environ.*, Vol.86 (2009), pp.63-68, Imagawa, H., Tanaka, T., Takahashi, N., Matsunaga, S., Suda, A. and Shinjoh, H., Titanium-doped Nanocomposite of Al₂O₃ and ZrO₂-TiO₂ as a Support with High Sulfur Durability for NO_x Storage-reduction Catalyst, © 2009 Elsevier, with permission from Elsevier.

Haruo Imagawa

Research Fields:

- Automotive Catalyst
- Storage Battery

Academic Societies:

- American Chemical Society
- Catalysis Society of Japan

